Regular Article

PHYSICAL CHEMISTRY RESEARCH
Published by the
Iranian Chemical Society
www.physchemres.org
info@physchemres.org

***Phys. Chem. Res.**, Vol. 6, No. 2, 415-431, June 2018*
DOI: 10.22036/pcr.2018.116937.1461

Fabrication of Magnetically Recoverable Nanocomposites by Combination of Fe_3O_4/ZnO with AgI and Ag_2CO_3: Substantially Enhanced Photocatalytic Activity under Visible Light

A. Habibi-Yangjeh* and B. Golzad-Nonakaran
Department of Chemistry, Faculty of Science, University of Mohaghegh Ardabili, P. O. Box: 179, Ardabil, Iran
(Received 26 January 2018, Accepted 1 April 2018)

We report highly efficient magnetically recoverable photocatalysts through combination of Fe_3O_4/ZnO with AgI and Ag_2CO_3, as narrow band gap semiconductors. The resultant photocatalysts were characterized by XRD, EDX, SEM. TEM, UV-Vis DRS, FT-IR, PL and VSM instruments. Under visible-light illumination, the nanocomposite with 1:6 weight ratio of Fe_3O_4 to ZnO/AgI/Ag_2CO_3 exhibited superior activity for degradation of RhB, which is nearly 20 and 11-folds higher than those of the Fe_3O_4/ZnO/Ag_2CO_3 and Fe_3O_4/ZnO/AgI photocatalysts, respectively. Furthermore, activity of this nanocomposite is 99 times higher than that of the Fe_3O_4/ZnO nanocomposite. The excellent activity of the nanocomposite was attributed to extended absorption in visible region and promoted separation of the charge carriers. Significantly, photocatalytic behavior of the nanocomposite was evaluated using photodegradations of three more organic pollutants and the highly improved activity in comparison to the counterparts was confirmed. Finally, the nanocomposite displayed enough magnetic properties to separate it using an external magnetic field.

Keywords: Fe_3O_4/ZnO/AgI/Ag_2CO_3, Magnetic photocatalyst, Water pollutants, Photodegradation

INTRODUCTION

Photocatalytic processes using semiconductors are promising technology to overcome various issues facing the human being in the field of environmental contamination, shortage of energy resources, and global warming of the earth [1-4]. During nearly four decades, various photocatalysts have been developed and their photocatalytic performances were studied mainly under UV and visible lights. As an abundant and green resource, it is straightforward to utilize the solar energy, as the light source, in photocatalytic processes [1-6]. Among the conventionally utilized photocatalysts, ZnO is the second popular photocatalyst [7,8]. This n-type semiconductor has a wide band gap of 3.20 eV [8]. Availability of precursors, environmentally benign, and high stability are some appealing properties of ZnO. Nonetheless, no absorption of visible light, fast recombination of the photoinduced electron/hole (e^-/h^+) pairs, and recovery of the utilized powders of the photocatalyst from the treated system seriously limit its widespread application in large scale [7-9]. Recovery of the utilized photocatalysts is still a time consuming and expensive step of the photocatalytic processes. Fortunately, magnetically recoverable photocatalysts offer a convenient pathway for facile separation of photocatalysts by applying magnetic fields [10]. These next generation of photocatalysts are synthesized by integration of a good magnetic material with photoactive semiconductors [10,11]. Elemental doping, integration with narrow band gap semiconductors, and combination with magnetic photocatalysts are the proposed strategies to handle these difficulties [12-19].

Among narrow band gap semiconductors, silver-containing semiconductors including Ag_2CO_3, Ag_3VO_4, Ag_3PO_4, AgBr, AgI and Ag_2CrO_4 have been combined with ZnO to enhance their visible-light absorption ability, which

*Corresponding author. E-mail: ahabibi@uma.ac.ir

is beneficial for improving the photocatalytic performance [20-25]. Very recently, it was displayed that by integration of two small band gap semiconductors with ZnO, one can fabricate more efficient visible-light-driven (VLD) photocatalysts [24,25]. Hence, in this work, we report combination of magnetically recoverable Fe_3O_4/ZnO (abbreviated as Mag/ZnO) nanocomposite with AgI and Ag_2CO_3 to fabricate novel magnetically recoverable efficient VLD photocatalyst. The nanocomposites were prepared by a simple ultrasonic-irradiation route using Fe_3O_4, zinc nitrate, silver nitrate, sodium hydroxide, sodium carbonate, and sodium iodide as precursors. The fabricated photocatalysts were extensively characterized by X-ray diffraction (XRD), scanning electron microscopy (SEM), transmission electron microscopy (TEM), energy dispersive analysis of X-rays (EDX), UV-Vis diffuse reflectance spectroscopy (DRS), Fourier transform-infrared (FT-IR) spectroscopy, and vibrating sample magnetometer (VSM). The as-obtained photocatalysts were used for degradations of rhodamine B (RhB), methylene blue (MB), methyl orange (MO) and fuchsine under visible-light illumination. Substantial improvement in the photocatalytic degradations of these pollutants over the Fe_3O_4/ZnO/AgI/Ag_2CO_3 (abbreviated as Mag/ZnO/AgI/AgCO) photocatalysts relative to the Mag/ZnO, Fe_3O_4/ZnO/AgI (abbreviated as Mag/ZnO/AgI), and Mag/ZnO/AgCO (abbreviated as Mag/ZnO/AgCO) was observed obviously. These enhancements were attributed to photosensitization of the nanocomposites to visible light and separation of the photoinduced charges due to the presence of AgI and Ag_2CO_3 semiconductors in the photocatalyst structure.

EXPERIMENTAL

Instruments

The XRD patterns of the synthesized photocatalysts were provided by a Philips Xpert X-ray diffractometer with Cu Kα radiation (λ = 0.15406 nm). Morphology of the photocatalysts was observed by LEO 1430VP SEM using an accelerating voltage of 15 kV and by a Zeiss-EM10C TEM instrument with an acceleration voltage of 80 kV. The purity and elemental analysis of the samples were explored by EDX system on the same SEM instrument. The UV-Vis DRS spectra were recorded by a Scinco 4100 apparatus. The FT-IR spectra were obtained by a Perkin Elmer Spectrum RX I apparatus. The PL spectra of the samples were studied using a Perkin Elmer (LS 55) fluorescence spectrophotometer. The UV-Vis spectra for the degradation reaction were plotted using a Cecile 9000 spectrophotometer. A Bandelin ultrasound processor of model HD 3100 (12 mm diameter Ti horn, 75 W, 20 kHz) was used for preparation of the photocatalysts.

Synthesis of the Photocatalysts

The Fe_3O_4 nanoparticles were fabricated by chemical co-precipitation method as reported by Massart [26]. For this purpose, in one beaker, 0.476 g $FeCl_3.6H_2O$ was dissolved in 20 ml of degassed water (solution A). In another beaker, 0.166 g $FeCl_2.4H_2O$ was dissolved in a solution containing 5 ml of degassed water and 0.8 ml of 2 mol dm^{-3} HCl (solution B). Then, solutions of A and B were added to each other under mechanical stirring and nitrogen degassing. Stirring of the suspension was continued for 30 min. Thereafter, aqueous ammonia (13.1 ml of 30% NH_3 at 250 ml of degassed water) was quickly added to the orange suspension under mechanical stirring. The resulting dark brown suspension was stirred for another 60 min and finally centrifuged to remove the precipitate and washed two times with water and ethanol and magnetically separated. The resultant precipitate was dried in an oven at 60 °C for 24 h.

The Mag/ZnO/AgI nanocomposite was prepared using ultrasonic irradiation by the procedure similar to our previous work [27]. For fabrication of the Mag/ZnO/AgI/AgCO (1:6) nanocomposite, where 1:6 is the weight ratio of Fe_3O_4 to ZnO/AgI/Ag_2CO_3, 0.454 g of the Mag/ZnO/AgI nanocomposite was dispersed in 150 ml of water by ultrasonic irradiation for 10 min by immersing the probe of the ultrasonic horn into the suspension in a cylindrical reactor provided with water circulation arrangement to maintain its temperature at 25 °C. Then, silver nitrate (0.061 g) was dissolved in the suspension and mechanically stirred for 60 min. After that, an aqueous solution of sodium carbonate (0.054 g in 20 ml of water) was slowly added to the formed suspension, and it was irradiated for 60 min. The suspension was centrifuged and the precipitate was washed twice with water and ethanol and dried in an oven at 60 °C for 24 h. For comparison purposes, the Mag/ZnO/AgCO and Mag/ZnO/AgI

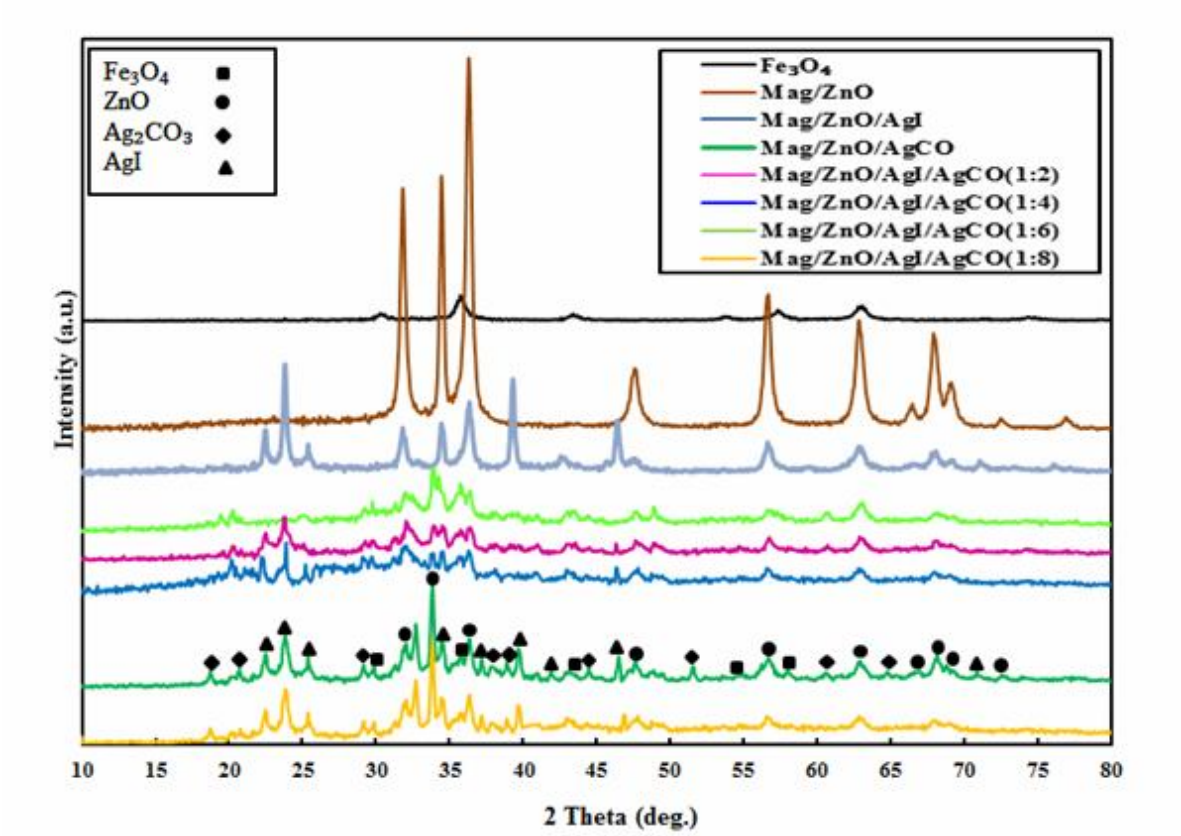

Fig. 1. XRD patterns for the Fe_3O_4, Mag/ZnO, Mag/ZnO/AgCO, Mag/ZnO/AgI and Mag/ZnO/AgI/AgCO nanocomposites with different weight percentages of silver carbonate.

nanocomposites were prepared with the same procedure.

Photocatalysis Experiments

The photocatalytic investigations were performed in a cylindrical reactor and its temperature was maintained at 25 °C using a water circulation system. The visible light was provided by a 50 W LED lamp positioned on the top of the photoreactor with distance of 20 cm from the solution. This source of light produces continues emission in visible region without any irradiations in UV and IR regions [28]. Before the light irradiation, a suspension containing 0.1 g of the photocatalyst and 250 ml aqueous solution of RhB (1×10^{-5} M), MB (1.3×10^{-5} M), MO (2.6×10^{-5}), or fuchsine (9.2×10^{-6}) was continuously stirred in dark for 60 min to attain equilibrium. Concentrations of the pollutants were analyzed by sampling from the reactor at regular intervals and the photocatalyst was removed before analysis by the spectrophotometer at 553, 664, 477 and 540 nm corresponding to the maximum absorption wavelengths of RhB, MB, MO and fuchsine, respectively.

RESULTS AND DISCUSSION

To observe crystallographic structure of the photocatalysts, their XRD patterns were provided. The XRD patterns of Fe_3O_4, Mag/ZnO, Mag/ZnO/AgCO, Mag/ZnO/AgI and Mag/ZnO/AgI/AgCO samples with different weight ratios of ZnO/AgI/AgCO to Fe_3O_4 are illustrated in Fig. 1. The diffraction peaks of Fe_3O_4 nanoparticles were perfectly indexed to the face-centered cubic crystalline phase (JCPDS file number of 75-1610) [28]. For the Mag/ZnO powder, diffraction peaks of ZnO with high intensity, which are the peaks of typical wurtzite hexagonal, and weak peaks of face-centered cubic

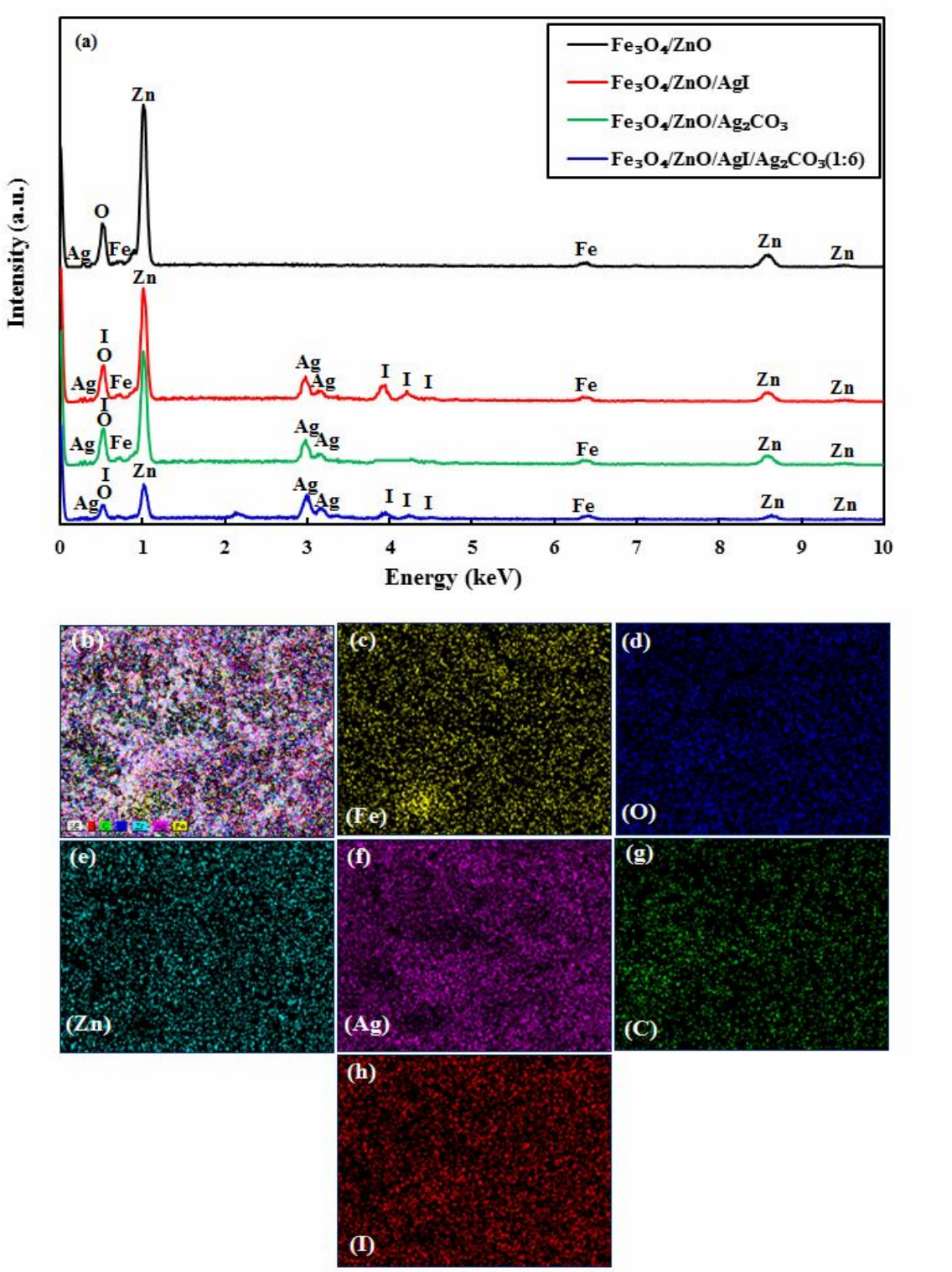

Fig. 2. (a) EDX spectra for the Mag/ZnO, Mag/ZnO/AgI, Mag/ZnO/AgCO and Mag/ZnO/AgI/AgCO (1:6) samples. (b)-(h) EDX mapping for the Mag/ZnO/AgI/AgCO (1:6) nanocomposite.

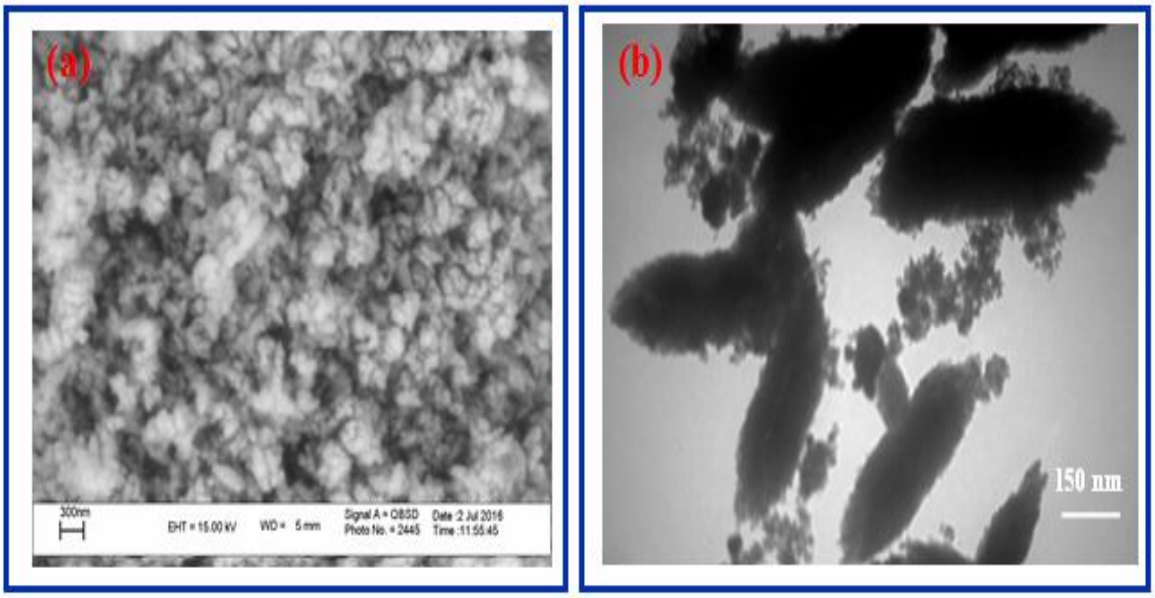

Fig. 3. (a) SEM and (b) TEM images for the Mag/ZnO/AgI/AgCO (1:6) nanocomposite.

crystalline phase of Fe_3O_4, are observed [29]. For the Mag/ZnO/AgI and Mag/ZnO/AgCO nanocomposites, in addition to the diffraction peaks of Fe_3O_4 and ZnO, the peaks for AgI (JCPDS 09-0374) [23] and Ag_2CO_3 (JCPDS 09-0374 and 78-0641) [30] are clearly observed, respectively. In the case of the Mag/ZnO/AgI/AgCO nanocomposites, the diffraction peaks for Fe_3O_4, ZnO, AgI, and Ag_2CO_3 are observed confirming preparation of the quaternary nanocomposites.

Composition of the synthesized photocatalysts was explored by the EDX analysis and the results are displayed in Fig. 2. As indicated in Fig. 2a, the Mag/ZnO nanocomposite shows the presence of Fe, Zn, and O elements, whereas the Mag/ZnO/AgI nanocomposite contains peaks for Fe, Zn, Ag, O and I elements. In addition, the Mag/ZnO/AgI/AgCO (1:6) nanocomposite is composed of Fe, Zn, Ag, O and C elements. Distribution of the elements in the Mag/ZnO/AgI/AgCO (1:6) nanocomposite was explored by elemental mapping technique and the results are displayed in Fig. 2b-h. The maps for Fe, Zn, Ag, O, I and C elements are well-defined with sharp contrast confirming the fabrication of the quaternary photocatalyst.

Figures 3a, b depicts the SEM and TEM images of the Mag/ZnO/AgI/AgCO (1:6) nanocomposite. As observed, the nanocomposite consists of mainly oval-like particles corresponding to ZnO and smaller nearly spherical particles of Fe_3O_4, AgI, and Ag_2CO_3 combined with the ZnO particles.

It is believed that light absorption properties of photocatalysts are of the key parameters affecting the photocatalytic performances. Thus, UV-Vis DRS spectra of the synthesized Mag/ZnO, Mag/ZnO/AgI/AgCO, Mag/ZnO/AgI and Mag/ZnO/AgI/AgCO nanocomposites with various compositions were provided, as presented in Fig. 4a. All of the photocatalysts showed strong absorption in the whole range of visible light. Especially, the Mag/ZnO/AgI/AgCO (1:6) nanocomposites displayed more pronounced absorption in this region and the absorption intensity slightly increased with loading more AgI/Ag_2CO_3 in the nanocomposites. Additionally, band gap energy (Eg) of the photocatalysts was calculated using Tauc's equation as $(\alpha h\nu)^2 = B(h\nu - Eg)$, where α, h, ν and B are absorption coefficient, Planck constant, light frequency, and a constant, respectively [31]. As observed in Fig. 4b, the estimated band gap energies of the photocatalysts are between 2.65 and 3.10 eV. Thus, the Mag/ZnO/AgI/AgCO nanocomposites have narrower band gaps and substantially

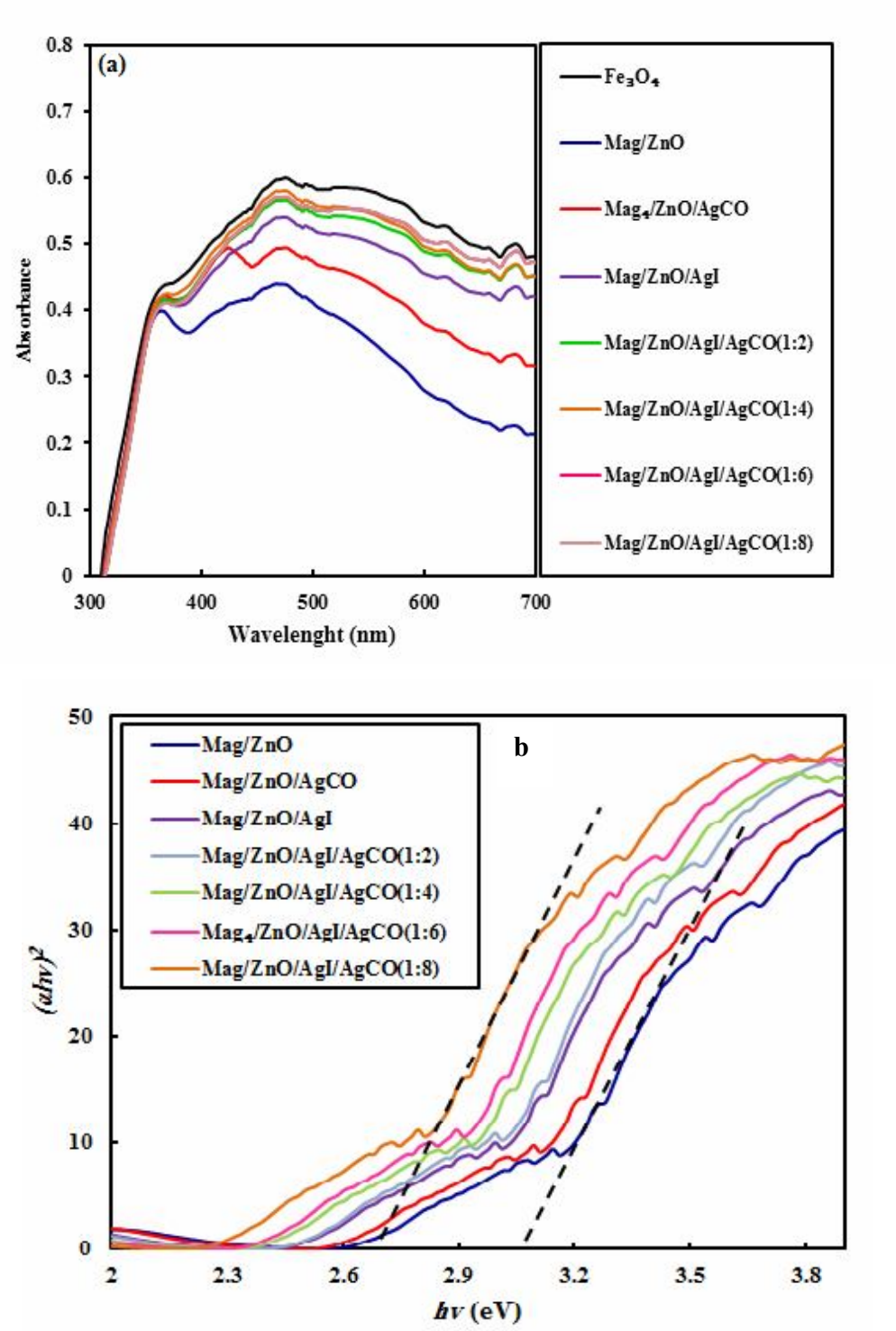

Fig. 4. (a) UV-Vis DRS for the Fe_3O_4, Mag/ZnO, Mag/ZnO/AgCO, Mag/ZnO/AgI and Mag/ZnO/AgI/AgCO nanocomposites with different compositions. (b) Plots of $(\alpha h\nu)^2$ versus $h\nu$ for the photocatalysts. (c) FT-IR spectra for the Fe_3O_4, Mag/ZnO, Mag/ZnO/AgCO, Mag/ZnO/AgI and Mag/ZnO/AgI/AgCO (1:6) samples.

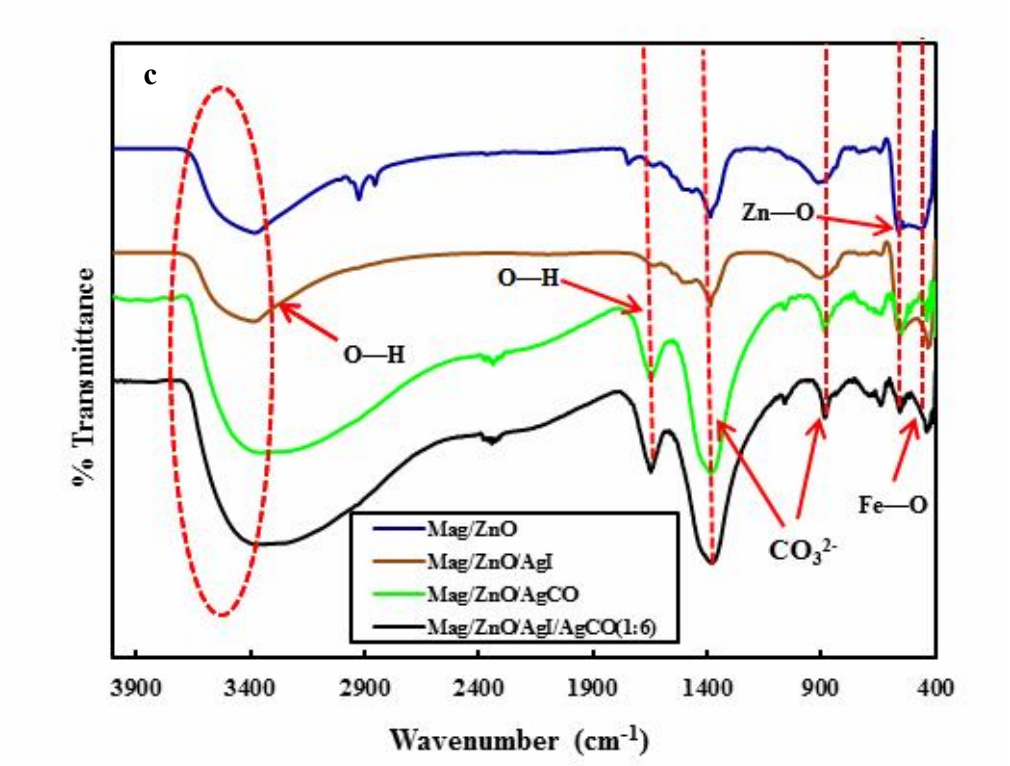

Fig. 4. Continued.

higher optical absorptions in visible region than the Mag/ZnO nanocomposite, which produce more charge carriers under visible light. Therefore, it is inferred that the Mag/ZnO/AgI/AgCO nanocomposites could have good VLD photocatalytic activity.

Chemical bonding and functional groups of the photocatalysts were studied using FT-IR spectroscopy and the spectra for Mag/ZnO, Mag/ZnO/AgCO, Mag/ZnO/AgI and Mag/ZnO/AgI/AgCO samples are illustrated in Fig. 4c. For these photocatalysts, the bands located at 573 cm^{-1} correspond to the Zn-O stretching vibration. The broad peaks at 3418-3450 cm^{-1} and the strong peaks at 1637 cm^{-1} are attributed to the stretching and bending vibrations of O-H group, belonging to the adsorbed water molecules [29]. For the Mag/ZnO/Ag_2CO_3 nanocomposite, the peaks appeared at 1386 and 887 cm^{-1} are attributed to the characteristic absorption peaks in the CO_3^{2-} group of Ag_2CO_3 [30]

The visible-light photocatalytic performances of different photocatalysts for RhB degradation are displayed in Fig. 5a. As seen, the dye solution under the light irradiation, without using any photocatalyst, has high stability, implying that it has considerable stability in this condition. Additionally, over the Mag/ZnO nanocomposite, photocatalytic degradation reaction of RhB is poor. Due to the presence of narrow band gap semiconductors, the Mag/ZnO/AgI and Mag/ZnO/AgCO nanocomposites show higher activity in comparison to the Mag/ZnO photocatalyst. Interestingly, the Mag/ZnO/AgI/AgCO nanocomposites exhibit substantial activity and the nanocomposite with 1:6 ratio of Fe_3O_4 to ZnO/AgI/AgCO shows extremely higher photocatalytic performance.

Figures 5b-d show the absorption spectra for degradation aqueous solutions of RhB over the Mag/ZnO, Mag/ZnO/AgCO, Mag/ZnO/AgI and Mag/ZnO/AgI/AgCO samples. Obviously, it is observed that the intensities of the absorption peaks continually decrease with prolonging the irradiation time without any changes in position of the peaks. This demonstrates aromatic skeleton breakage of RhB under the light irradiation. After the light irradiation

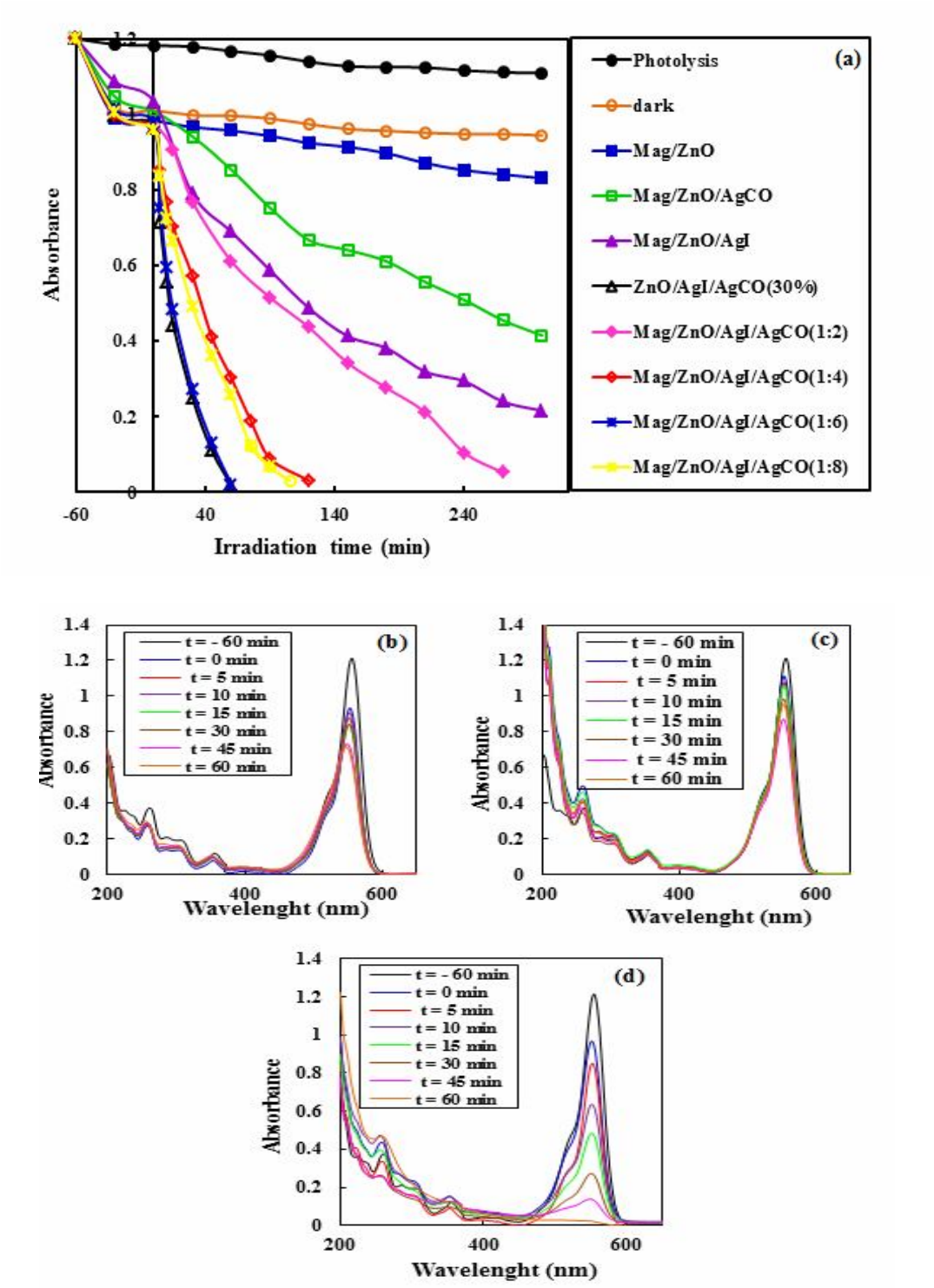

Fig. 5. (a) Photodegradation of RhB over the Mag/ZnO, Mag/ZnO/AgCO, Mag/ZnO/AgI and Mag/ZnO/AgI/AgCO (1:6) nanocomposites. UV-Vis spectra for degradation of RhB under visible-light irradiation over the (b) Mag/ZnO /AgCO, (c) Mag/ZnO/AgI and (d) Mag/ZnO/AgI/AgCO (1:6) nanocomposite.

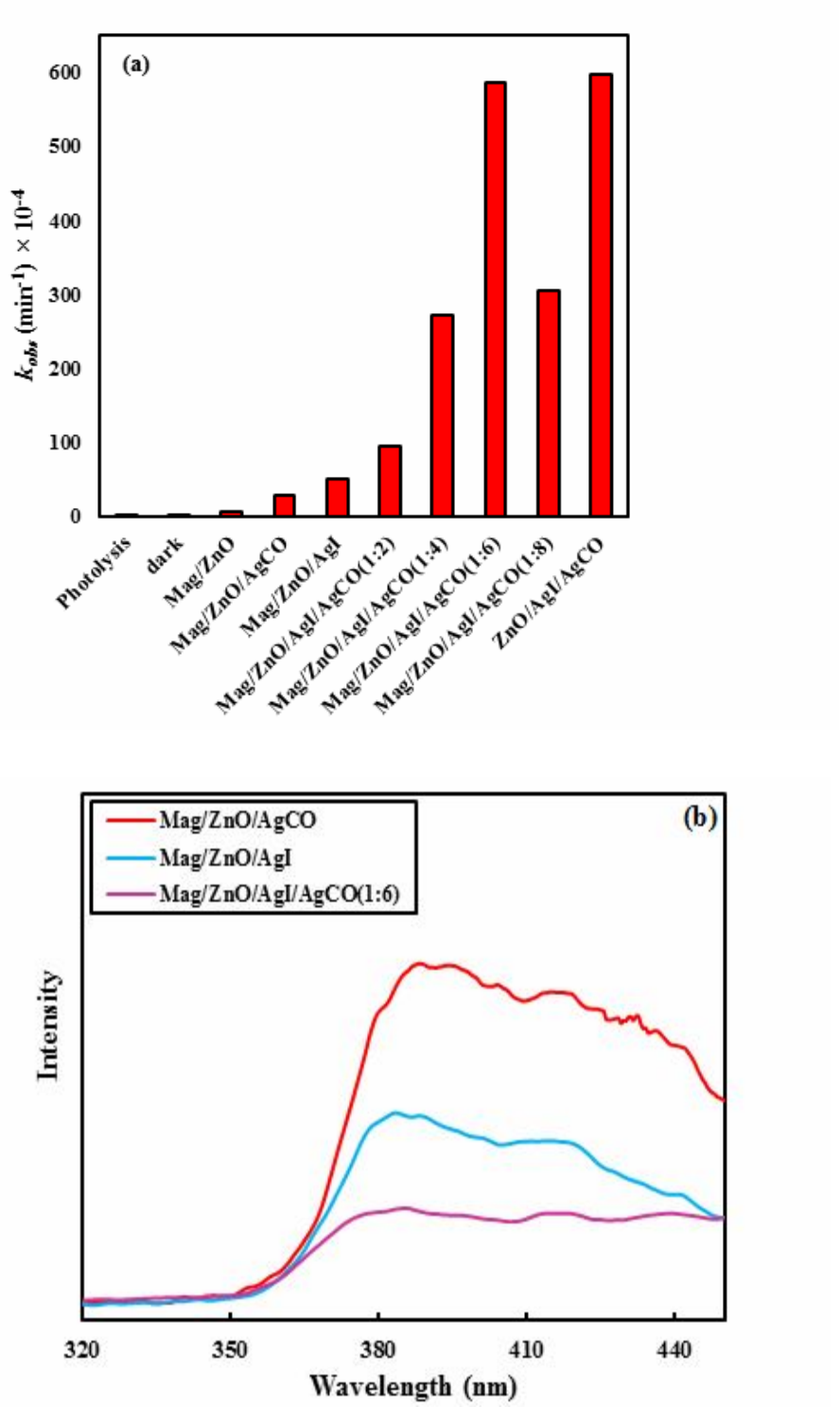

Fig. 6. (a) The degradation rate constants of RhB over the Mag/ZnO, Mag/ZnO/AgCO, Mag/ZnO/AgI and Mag/ZnO/AgI/AgCO nanocomposites. (b) PL spectra for the Mag/ZnO/AgCO, Mag/ZnO/AgI and Mag/ZnO/AgI/AgCO (1:6) nanocomposites.

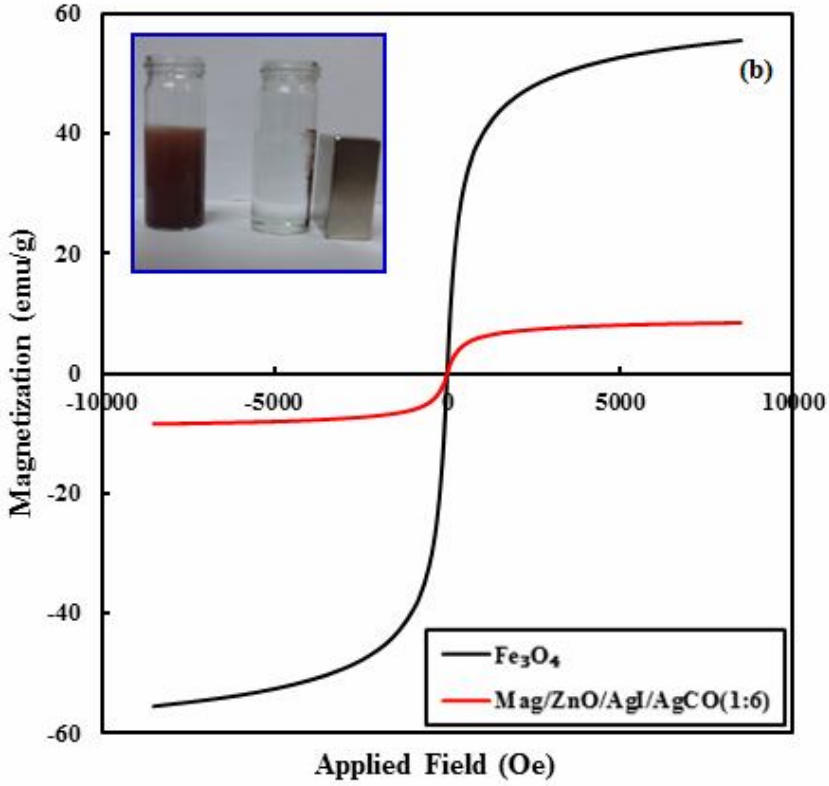

Fig. 7. Magnetization curves for the Fe_3O_4 nanoparticles and Mag/ZnO/AgI/AgCO (1:6) nanocomposite. Inset of the figure shows the photograph for separation process by using a magnet.

for 70 min, about 36%, 59% and 96% of RhB molecules were degraded over the Mag/ZnO/AgCO, Mag/ZnO/AgI, and Mag/ZnO/AgI/AgCO samples, respectively.

The degradation rate constants of RhB on the synthesized photocatalysts are displayed in Fig. 6a. It is clear that the degradation rate constant increases with weight ratio of Fe_3O_4 to ZnO/AgI/AgCO up to 1:6 and the activity of Mag/ZnO/AgI/AgCO (1:8) nanocomposite is lower than that of the Mag/ZnO/AgI/AgCO (1:6) photocatalyst. Photocatalytic performance of the Mag/ZnO/AgI/AgCO (1:6) nanocomposite is almost 99 times faster than that of the Mag/ZnO, 11 times faster than that of the Mag/ZnO/AgI, and 20 times faster than that of the Mag/ZnO/AgCO photocatalysts. The PL analysis was used to estimate the photoinduced charge carrier separation of the photocatalysts. It is well believed that the higher PL intensity indicates the faster recombination rate of the charge carriers, resulting in lower photocatalytic activity [9]. The PL spectra for the Mag/ZnO/AgI, Mag/ ZnO/Ag_2CO_3, and Mag/ZnO/AgI/AgCO (1:6) samples were provided and the results are displayed in Fig. 6b. As can be seen, the Mag/ZnO/AgI/AgCO (1:6) nanocomposite exhibits the emission peak located at almost the same position of the Mag/ZnO/AgI and Mag/ZnO/Ag_2CO_3 photocatalysts, but with substantially decreased emission intensity, suggesting that the Mag/ZnO/AgI/AgCO (1:6) nanocomposite has much lower recombination rate for the photoinduced charge carriers. Thus, recombination of the charge carriers was greatly suppressed in the Mag/ZnO/AgI/AgCO (1:6) nanocomposite, resulting in highly improved activity

Figure 7 shows magnetization curve for the Fe_3O_4 and Mag/ZnO/AgI/AgCO (1:6) samples, which exhibits super paramagnetic behavior with a very low coercivity and a saturation magnetizations of 55.5 and 8.35 emu g^{-1}, respectively. As the inset of Fig. 6c displays, the nanocomposite is simply recovered from the treated system

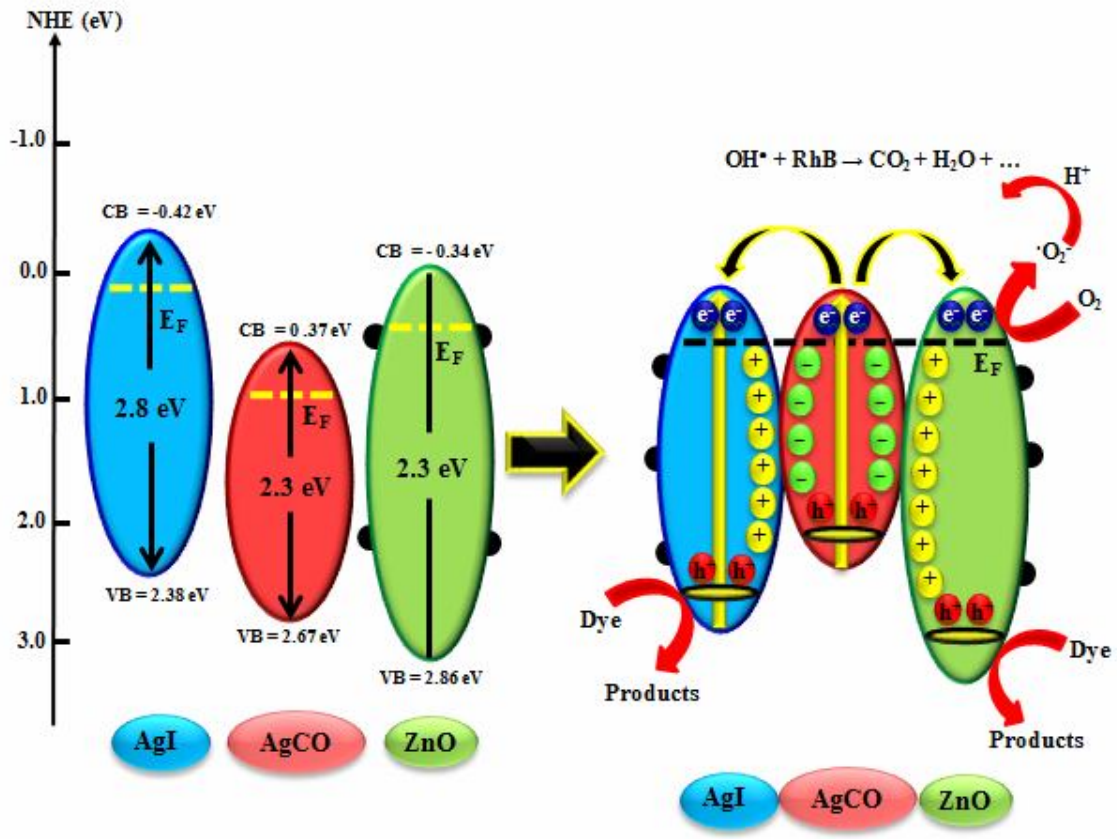

Fig. 8. A plausible diagram for separation of electron-hole pairs in the Mag/ZnO/AgI/AgCO nanocomposites.

using a magnet, implying that saturation magnetizations is enough for magnetically recovering of the photocatalyst.

Through the above discussions, the possible photocatalytic mechanism for the enhanced VLD photoactivity of the Mag/ZnO/AgI/AgCO nanocomposites was proposed (Fig. 8). The conduction band (CB) potentials of ZnO, AgI, and Ag_2CO_3 are -0.34, -0.42 and +0.37 eV, respectively, whereas the valence band (VB) potentials are +2.86, +2.38 and +2.67 eV [30]. After junction of the counterparts, electrons freely move from ZnO and AgI to Ag_2CO_3, because Fermi energy level of Ag_2CO_3 is lower than those of ZnO and AgI. Therefore, due to n-type characteristics of ZnO, AgI and Ag_2CO_3 semiconductors, tandem n-n heterojunctions are formed between these semiconductors [32]. These heterojunctions induce internal charges in the junction places directed from AgI and ZnO to Ag_2CO_3. Illumination of visible light produces e^-/h^+ pairs in AgI and Ag_2CO_3 semiconductors, because of their small band gaps. As confirmed by PL analysis, the photogenerated electrons strongly migrate from Ag_2CO_3 to AgI and ZnO, which is useful for separation of the charge carriers. Meanwhile, the photogenerated holes in the VB of AgI move to the VB of Ag_2CO_3. For this reason, highly improved photocatalytic performance was observed for the Mag/ZnO/AgI/AgCO nanocomposites. Additionally, RhB absorbs some of photons from visible light and subsequently electrons are excited from its HOMO to LUMO orbitals. After that, electrons transfer from RhB to the CB of ZnO, Ag_2CO_3, and AgI. The transferred electrons generate different reactive species in the next steps [33].

It is generally accepted that in photocatalytic reactions a series of photoinduced reactive species such as hydroxyl radicals ($^{\bullet}OH$), holes (h^+) and superoxide anion radicals ($^{\bullet}O^-_2$) are responsible for the degradation reactions [9,11].

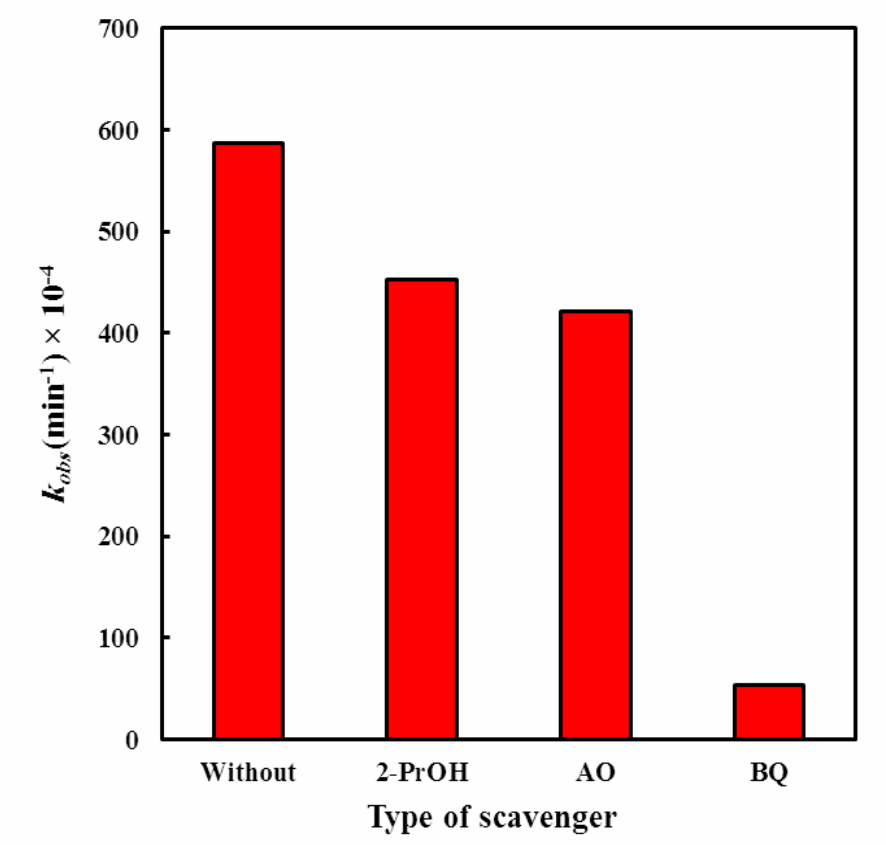

Fig. 9. The degradation rate constants of RhB over the Mag/ZnO/AgI/AgCO (1:6) nanocomposite in presence of various scavengers**.**

To determine the role of these species, the degradation reaction over the Mag/ZnO/AgI/AgCO (1:6) nanocomposite was performed in the presence of benzoquinone, ammonium oxalate and 2-propanol as the scavengers for $^{\bullet}O_2^-$, h^+, and $^{\bullet}OH$ species and the results are shown in Fig. 9. It was found that the degradation rate constant in the absence of scavengers (587 × 10^{-4} min^{-1}) has been decreased to 452 × 10^{-4}, 421 × 10^{-4} and 54.3 × 10^{-4} min^{-1} in the presence of 2-propanol, ammonium oxalate and benzoquinone, respectively. Obviously, the introduction of benzoquinone caused a remarkable decrease in the photocatalytic activity, whereas in the presence of ammonium oxalate and 2-propanol, the degradation reactions were not substantially inhibited. Thus, direct superoxide anion radical oxidation has a major role in the degradation reaction relative to the holes and hydroxyl radicals.

In order to display the degradation performance of the Mag/ZnO/AgI/AgCO (1:6) nanocomposite in photodegradations of other pollutants, MB, MO and fuchsine dyes were selected and the rate constants are shown in Fig. 10. It is evident that activity of the Mag/ZnO/AgI/AgCO (1:6) nanocomposite in degradations of these pollutants are substantially larger than those of the Mag/ZnO, Mag/ZnO/AgI and Mag/ZnO/AgCO nanocomposites. As observed, by coupling certain amounts of Ag_2CO_3 and AgI to Mag/ZnO, the photocatalytic activity considerably enhances. The photocatalytic performance of Mag/ZnO/AgI/AgCO (1:6) nanocomposite for degradation of MB is about 48.9, 10.5 and 9.4-folds larger than those of the Mag/ZnO, Mag/ZnO/AgCO, and Mag/ZnO/AgI samples, respectively, whereas the activity in degradations of MO is about 19.5, 9.8 and 4.9 folds greater. In addition, photocatalytic activity of the quaternary nanocomposite in degradation of fuchsine is about 106, 13.2

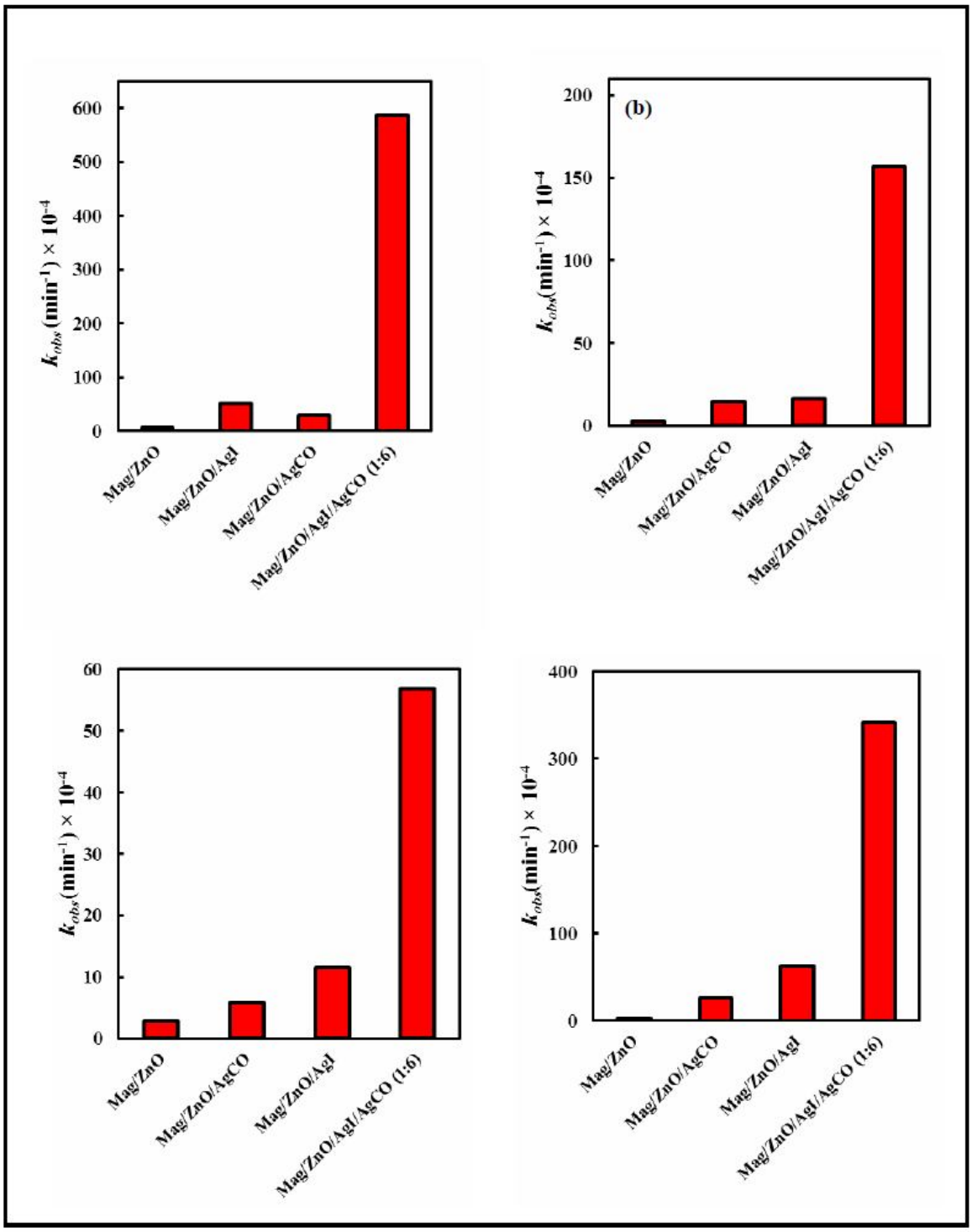

Fig. 10. The degradation rate constants of (a) RhB, (MB), (MO), and (d) fuschine over the ZnO/Mag, Mag/ZnO/AgCO, Mag/ZnO/AgI and Mag/ZnO/AgI/AgCO (1:6) samples under visible-light irradiation.

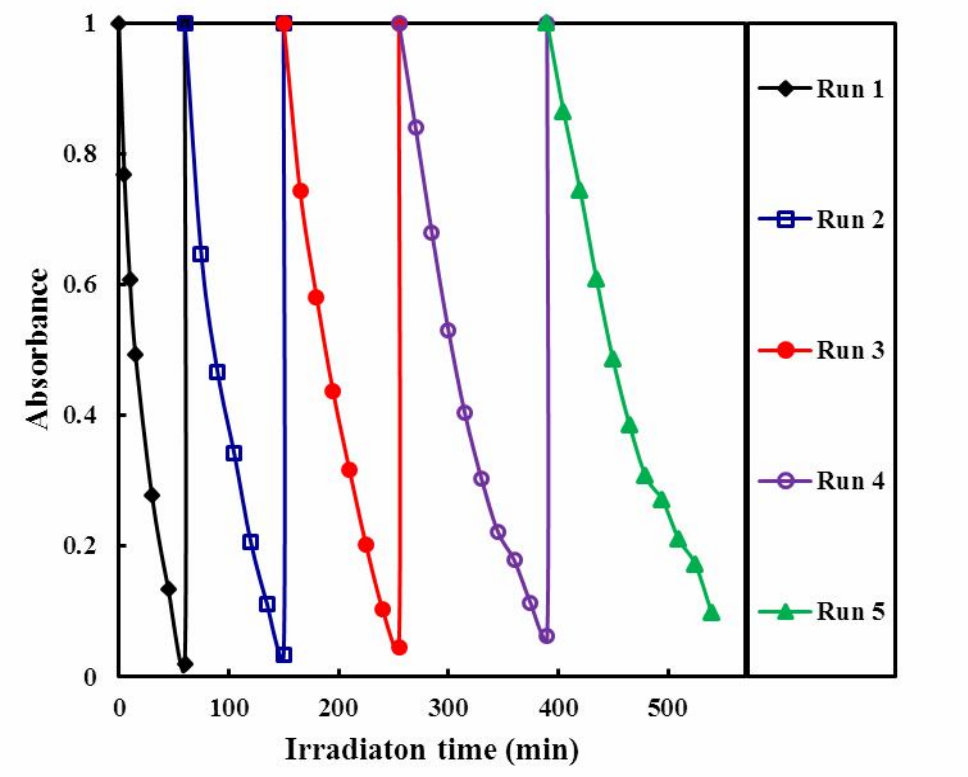

Fig. 11. Reusability of the Mag/ZnO/AgI/AgCO (1:6) nanocomposite.

and 5.4-folds greater than those of the Mag/ZnO, Mag/ZnO/AgCO and Mag/ZnO/AgI samples, respectively. Thus, it was concluded that the photocatalyst has highly improved activity in removal of various contaminants.

Finally, reusability of the Mag/ZnO/AgI/AgCO (1:6) nanocomposite was tested in degradation of RhB under visible light for five runs and the results are displayed in Fig. 10. The photocatalyst was recovered after each cycle by centrifugation and dried at 80 °C for 24 h and then reused. As shown, after five cycles, the photocatalytic efficiency decreased only slightly compared to the first runs, implying that the photocatalyst has good potential to apply for the environmental remediation purposes.

CONCLUSIONS

In summary, we synthesized the Mag/ZnO/AgI/AgCO nanocomposites by facile consecutive combining AgI and Ag_2CO_3 with the Mag/ZnO nanocomposite. The as-synthesized Mag/ZnO/AgI/AgCO nanocomposites showed substantial VLD photocatalytic performance in degradations of RhB, MB, MO, and fuchsine in comparison with their counterparts. The Mag/ZnO/AgI/AgCO (1:6) nanocomposite displayed superior activity, which are 99, 11 and 20-folds higher than the Mag/ZnO, Mag/ZnO/AgI and Mag/ZnO/AgCO nanocomposites in degradation of RhB, respectively, whereas nearly 49, 10 and 9-folds in degradation of MB. This greatly improved photocatalytic performance was attributed to the efficient separation of the photoinduced charge carriers and substantial absorption of visible light, due to formation of heterojunction between ZnO and two small band gap semiconductors, which was confirmed by PL analysis. The trapping experiments exhibited that superoxide anion radicals have a key role in the degradation reaction. Investigation about magnetic properties displayed that the quaternary photocatalyst has enough saturation magnetization to be separated by applying magnetic field. Finally, recycling testes showed

that the photocatalyst has a considerable stability during five runs.

REFERENCES

[1] Dong, S.; Feng, J.; Fan, M.; Pi, Y.; Hu, L.; Han, X.; Liu, M.; Sun, J.; Sun, J., Recent developments in heterogeneous photocatalytic water treatment using visible light-responsive photocatalysts: A review. *RSC Advances* **2015**, *5*, 14610-14630, DOI: 10.1039/C4RA13734E.

[2] Bora, L. V.; Mewada, R. K., Visible/solar light active photocatalysts for organic effluent treatment: Fundamentals, mechanisms and parametric review, *Renewable and Sustainable Energy Reviews* **2017**, *76*, 1393-1421, DOI: 10.1016/ j.rser.2017.01.130.

[3] Chen, Y.; Jia, G.; Hu, Y.; Fan, G.; Tsang, Y. H.; Li, Z.; Zou, Z., Two-dimensional nanomaterials for photocatalytic CO_2 reduction to solar fuels. *Sustainable Energy Fuels* **2017**, *1*, 1875-1898, DOI: 10.1039/C7SE00344G.

[4] Zhang, G.; Lan, Z.-A.; Wang, X.; The surface engineering of graphitic carbon nitride polymers with cocatalysts for photocatalytic overall water splitting, *Chem. Sci.* **2017**, *8*, 5261-5274, DOI: 10.1039/C7SC01747B.

[5] Wu, Z.; Yuan, X.; Wang, H.; Wu, Z.; Jiang, L.; Wang, L.; Zhang, L.; Xiao, Z.; Chen, X.; Zeng, G., Facile synthesis of a novel full-spectrum-responsive Co2.67S4 nanoparticles for UV- Vis- and NIR-driven photocatalysis, *Appl. Catal. B: Environ.* **2017**, *202*, 104-111, DOI: 10.1016/ j.apcatb.2016.08.064.

[6] Wu, Y.; Wang, H.; Tu, W.; Liu, Y.; Tan, Y. Z.; Yuan, X.; Chew, J. W., Quasi-polymeric construction of stable perovskite-type $LaFeO_3$/g-C3N4 heterostructured photocatalyst for improved Z-scheme photocatalytic activity via solid p-n heterojunction interfacial effect, *J. Hazard. Mater.* **2018**, *347*, 412-422, DOI: 10.1016/ j.jhazmat.2018.01.025.

[7] Lee, K. M.; Lai, C. W.; Ngai, K. S.; Juan, J. C., Recent developments of zinc oxide based photocatalyst in water treatment technology: A review. *Water Res.* **2016**, *88*, 428-448, DOI: 10.1016/j.watres.2015.09.045.

[8] Girish Kumar, G.; K. S. R.; Koteswara Rao, K., Comparison of modification strategies towards enhanced charge carrier separation and photocatalytic degradation activity of metaloxide semiconductors (TiO_2, WO_3 and ZnO), *Appl. Surf. Sci.* **2017**, *391*, 124-148, DOI: 10.1016/ j.apsusc.2016.07.081.

[9] Pirhashemia, M.; Habibi-Yangjeh, A.; Rahim Pouranb, S., Review on the criteria anticipated for the fabrication of highly efficient ZnO-based visible-light-driven photocatalysts, *J. Indust. Eng. Chem.* **2018**, *62*, 1-25, DOI: 10.1016/ j.jiec.2018.01.012.https://doi.org/10.1016/j.jhazmat. 2018.01.025.

[10] Gómez-Pastora, J.; Dominguez, S.; Bringas, E.; Rivero, M. J.; Ortiz, I.; Dionysiou, D. D., Review and perspectives on the use of magnetic nanophotocatalysts (MNPCs) in water treatment, *Chem. Eng. J.* **2017**, *310*, 407-427, DOI: 10.1016/j.cej.2016.04.140.

[11] Mousavi, M.; Habibi-Yangjeh, A.; Rahim Pouran, S., Review on magnetically separable graphitic carbon nitride-based nanocomposites as promising visible-light-driven photocatalysts, *J. Mater. Sci.: Mater Electron.* **2018**, *29*, 1719-1747, DOI: 10.1007/s10854-017-8166-x.

[12] Kulkarni, S. D.; Kumbar, S. Menon, S. G.; Choudhari, K. S.; Santhosh, C., Magnetically separable core-shell $ZnFe_2O_4$@ZnO nanoparticles for visible light photodegradation of methyl orange, *Mater. Res. Bull.* **2016**, *77*, 70-77, DOI: 10.1016/ j.materresbull.2016.01.022.

[13] Pirhashemi, M.; Habibi-Yangjeh, A.; Ultrasonic-assisted preparation of plasmonic ZnO/Ag/Ag_2WO_4 nanocomposites with high visible-light photocatalytic performance for degradation of organic pollutants, *J. Colloid Interf. Sci.* **2017**, *491*, 216-229, DOI: 10.1016/j.jcis.2016.12.044.

[14] Luo, Q.; Yang, Y.; Zhao, X.; Wang, D.; Yin, R.; Li, X.; An, J., Facile preparation of well-dispersed ZnO/cyclized polyacrylonitrile nanocomposites with

highly enhanced visible-light photocatalytic activity, *Appl. Catal. B: Environ*. **2017**, *204*, 304-315, DOI: 10.1016/j.apcatb.2016.11.037.

[15] Lamba, R.; Umar, A.; Mehta, S. K.; Kansal, S. K., Enhanced visible light driven photocatalytic application of Ag_2O decorated ZnO nanorods heterostructures, *Sep. Purif. Technol.* **2017**, *183*, 341-349, DOI: 10.1016/j.seppur.2017.03.070, DOI: 10.1016/j.seppur.2017.03.070.

[16] Jiang, J.; Wang, H.; Chen, X.; Li, S.; Xie, T.; Wang, D.; Lin, Y., Enhanced photocatalytic degradation of phenol and photogenerated charges transfer property over BiOI-loaded ZnO composites, *J. Colloid Interf. Sci.* **2017**, *494*, 130-138, DOI: 10.1016/j.jcis.2017.01.064.

[17] Senthil Kumar, P.; Selvakumar, M.; Ganesh Babu, S.; Induja, S.; Karuthapandian, S., CuO/ZnO nanorods: An affordable efficient p-n heterojunction and morphology dependent photocatalytic activity against organic contaminants, *J. Alloys Compd.* **2017**, 701, 562-573, DOI: 10.1016/j.jallcom.2017.01.126.

[18] Reda, G. M.; Fan, H.; Tian, H.; Room-temperature solid state synthesis of Co_3O_4/ZnO p-n heterostructure and its photocatalytic activity, *Adv. Powder Technol.* **2017**, *28*, 953-963, DOI: 10.1016/j.apt.2016.12.025.

[19] Chen, Q.; Hou, H.; Zhang, D.; Hu, S.; Min, T.; Liu, B.; Yang, C.; Pu, W.; Hu, J.; Yang, J., Enhanced visible-light driven photocatalytic activity of hybrid ZnO/g-C_3N_4 by high performance ball milling, *J. Photochem. Photobiol. A: Chem.* **2018**, *350*, 1-9, DOI: 10.1016/j.jphotochem.2017.09.015, DOI: 10.1016/j.jphotochem.2017.09.015.

[20] Dong, C.; Wu, K. -L.; Li, M. -R.; Liu, L.; Wei, X. -W.; Synthesis of Ag_3PO_4-ZnO nanorod composites with high visible-light photocatalytic activity, *Catal. Commun.* **2014**, *46*, 32-35, DOI: 10.1016/j.catcom.2013.11.018.

[21] Wu, C., Synthesis of Ag_2CO_3/ZnO nanocomposite with visible light-driven photocatalytic activity, *Mater. Lett.* **2014**, *136*, 262-264, DOI: 10.1016/j.matlet.2014.08.074.

[22] Naghizadeh-Alamdari, S.; Habibi-Yangjeh, A., Sonochemical preparation of AgBr-ZnO nanocomposites in water using one-pot method as highly efficient photocatalysts under visible light, *J. Iran. Chem. Soc.* **2015**, *12*, 1961-1971, DOI: 10.1007/s1373.

[23] Shaker-Agjekandy, S.; Habibi-Yangjeh, A., Facile one pot method for preparation of AgI/ZnO nanocomposites as visible-light-driven photocatalysts with enhanced activities, *Mater. Sci. Semicond. Process.* **2015**, *24*, 74-81, DOI: 10.1016/j.mssp.2015.02.022.

[24] Golzad-Nonakaran, B; Habibi-Yangjeh, A., Photosensitization of ZnO with Ag_3VO_4 and AgI nanoparticles: Novel ternary visible-light-driven photocatalysts with highly enhanced activity, *Adv. Powder Technol.* **2016**, *27*, 1427-1437, DOI: 10.1016/j.apt.2016.05.001.

[25] Chen, C.; Li, Z.; Lin, H.; Wang, G.; Liao, J.; Li, M.; Lv, S.; Li, W., Enhanced visible light photocatalytic performance of ZnO nanowires integrated with CdS and Ag_2S, *Dalton Trans.* **2016**, *45*, 3750-3758, DOI: 10.1039/C5DT04533A.

[26] Massart, R., Preparation of aqueous magnetic liquids in alkaline and acidic media. *IEEE Trans. Magn.* **1981**, *17*, 1247-1248, DOI: 10.1109/TMAG.1981.1061188.

[27] Shekofteh-Gohari, M.; Habibi-Yangjeh, A., Ultrasonic-assisted preparation of novel ternary ZnO/AgI/Fe_3O_4 nanocomposites as magnetically separable visible-light-driven photocatalysts with excellent activity, *J. Colloid Interf. Sci.* **2016**, *461*, 144-153, DOI: 10.1016/j.jcis.2015.09.032.

[28] Shekofteh-Gohari, M.; Habibi-Yangjeh, A., Facile preparation of Fe_3O_4@AgBr-ZnO nanocomposites as novel magnetically separable visible-light-driven photocatalysts, *Ceram. Int.* **2015**, *41*, 1467-1476, DOI: 10.1016/j.ceramint.2014.09.081.

[29] Shekofteh-Gohari, M.; Habibi-Yangjeh, A., Novel magnetically separable Fe_3O_4@ZnO/AgCl nanocomposites with highly enhanced photocatalytic activities under visible-light irradiation, *Sep. Purif. Technol.* **2015**, *147*, 194-202, DOI: 10.1016/j.seppur.2015.04.034.

[30] Golzad-Nonakaran, B; Habibi-Yangjeh, A., Ternary

$ZnO/AgI/Ag_2CO_3$ nanocomposites: Novel visible-light-driven photocatalysts with excellent activity in degradation of different water pollutants, *Mater. Chem. Phys.* **2016**, *184*, 210-221, DOI: 10.1016/j.matchemphys.2016.09.044.

[31] Li, X.; Ye, J., Photocatalytic degradation of rhodamine B over $Pb_3Nb_4O_{13}$/fumed SiO_2 composite under visible light irradiation, *J. Phys. Chem. C* **2007**, *111*, 13109-13116, DOI: 10.1021/jp072752m.

[32] Pirhashemi, M.; Habibi-Yangjeh, A., Photosensitization of ZnO by AgBr and Ag_2CO_3: Nanocomposites with tandem n-n heterojunctions and highly enhanced visible-light photocatalytic activity, *J. Colloid Interf. Sci.* **2016**, *474*, 103-113, DOI: 10.1016/j.jcis.2016.04.022.

[33] Pirhashemi, M.; Habibi-Yangjeh, A., Ultrasonic-assisted preparation of plasmonic $ZnO/Ag/Ag_2WO_4$ nanocomposites with high visible-light photocatalytic performance for degradation of organic pollutants, *J. Colloid Interf. Sci.* **2017**, *491*, 216-229, DOI: 10.1016/j.jcis.2016.12.044.